

# Online Research @ Cardiff

This is an Open Access document downloaded from ORCA, Cardiff University's institutional repository: <https://orca.cardiff.ac.uk/id/eprint/122393/>

This is the author's version of a work that was submitted to / accepted for publication.

Citation for final published version:

Liu, Chuangchuang, Sun, Xianfang ORCID: <https://orcid.org/0000-0002-6114-0766>, Chen, Changyou, Rosin, Paul ORCID: <https://orcid.org/0000-0002-4965-3884>, Yan, Yitong, Jin, Longcun and Pen, Xinyi 2019. Multi-scale residual hierarchical dense networks for single image super-resolution. IEEE Access 7 , 60572 -60583. 10.1109/ACCESS.2019.2915943 file

Publishers page: <http://dx.doi.org/10.1109/ACCESS.2019.2915943>  
<<http://dx.doi.org/10.1109/ACCESS.2019.2915943>>

Please note:

Changes made as a result of publishing processes such as copy-editing, formatting and page numbers may not be reflected in this version. For the definitive version of this publication, please refer to the published source. You are advised to consult the publisher's version if you wish to cite this paper.

This version is being made available in accordance with publisher policies.

See

<http://orca.cf.ac.uk/policies.html> for usage policies. Copyright and moral rights for publications made available in ORCA are retained by the copyright holders.



Date of publication xxxx 00, 0000, date of current version xxxx 00, 0000.

Digital Object Identifier 10.1109/ACCESS.2017.DOI

# Multi-scale Residual Hierarchical Dense Networks for Single Image Super-Resolution

CHUANGCHUANG LIU<sup>1</sup>, XIANFANG SUN<sup>2</sup>, CHANGYOU CHEN<sup>3</sup>, PAUL L. ROSIN<sup>2</sup>, YITONG YAN<sup>1</sup>, LONGCUN JIN<sup>1</sup> (Member, IEEE), XINYI PENG<sup>1</sup>

<sup>1</sup>School of Software Engineering, South China University of Technology, Guangzhou, China

<sup>2</sup>School of Computer Science and Informatics Cardiff University, UK

<sup>3</sup>Department of Computer Science and Engineering, University at Buffalo, State University of New York, NY, USA

Corresponding author: Longcun Jin (e-mail: lcjin@scut.edu.cn).

**ABSTRACT** Single image super-resolution is known to be an ill-posed problem, which has been studied for decades. With the developments of deep convolutional neural networks, the CNN-based single image super-resolution methods have greatly improved the quality of the generated high-resolution images. However, it is difficult for image super-resolution to make full use of the relationship between pixels in low-resolution images. To address this issue, we propose a novel multi-scale residual hierarchical dense network, which tries to find the dependencies in multi-level and multi-scale features. Specially, we apply the atrous spatial pyramid pooling, which concatenates multiple atrous convolutions with different dilation rates, and design a residual hierarchical dense structure for single image super-resolution. The atrous-spatial-pyramid-pooling module is used for learning the relationship of features at multiple scales; while the residual hierarchical dense structure, which consists of several hierarchical dense blocks with skip connections, aims to adaptively detect key information from multi-level features. Meanwhile, dense features from different groups are connected in a dense approach by hierarchical dense blocks, which can adequately extract local multi-level features. Extensive experiments on benchmark datasets illustrate the superiority of our proposed method compared with state-of-the-art methods. The super-resolution results on benchmark datasets of our method can be downloaded from <https://github.com/Rainyfish/MS-RHDN>, and the source code will be released upon acceptance of the paper.

**INDEX TERMS** Convolutional neural networks, deep learning, multi-scale residual hierarchical dense, image super-resolution

## I. INTRODUCTION

**S**INGLE image super-resolution (SISR) aims to reconstruct a high-resolution (HR) image from its low-resolution (LR) version. Image super-resolution is widely used in many computer vision fields, such as video surveillance, remote sensing, and image sensing. However, SISR is a typically ill-posed problem as the image degradation process is usually irreversible and lots of tiny textures are missing in LR images. Several high-resolution images can be potentially generated from a given LR image. Recently, deep convolutional neural networks have been applied in many tasks, ranging from low-level (image restoration, SISR, etc.) to high-level (image classification, object detection, etc.) vision fields, and have shown great improvements compared

with conventional methods.

Currently, CNN-based SISR methods, which learn an effective nonlinear mapping function from LR images to HR images directly, have greatly improved the quality of the super-resolved image. Among them, Dong et al. [1] firstly used a deep convolutional neural network called SRCNN, consisting of three convolutional layers, to address the SISR problem. Since then, lots of deep-learning SISR methods have been developed. VDSR [2] provides remarkable performance by increasing the depth of the network to 20, proving the importance of the network depth for detecting effective features of images. SRCNN and VDSR involve the interpolated images for pre-processing, whose spatial size is the same as the HR images. FSRNN [3] was proposed to

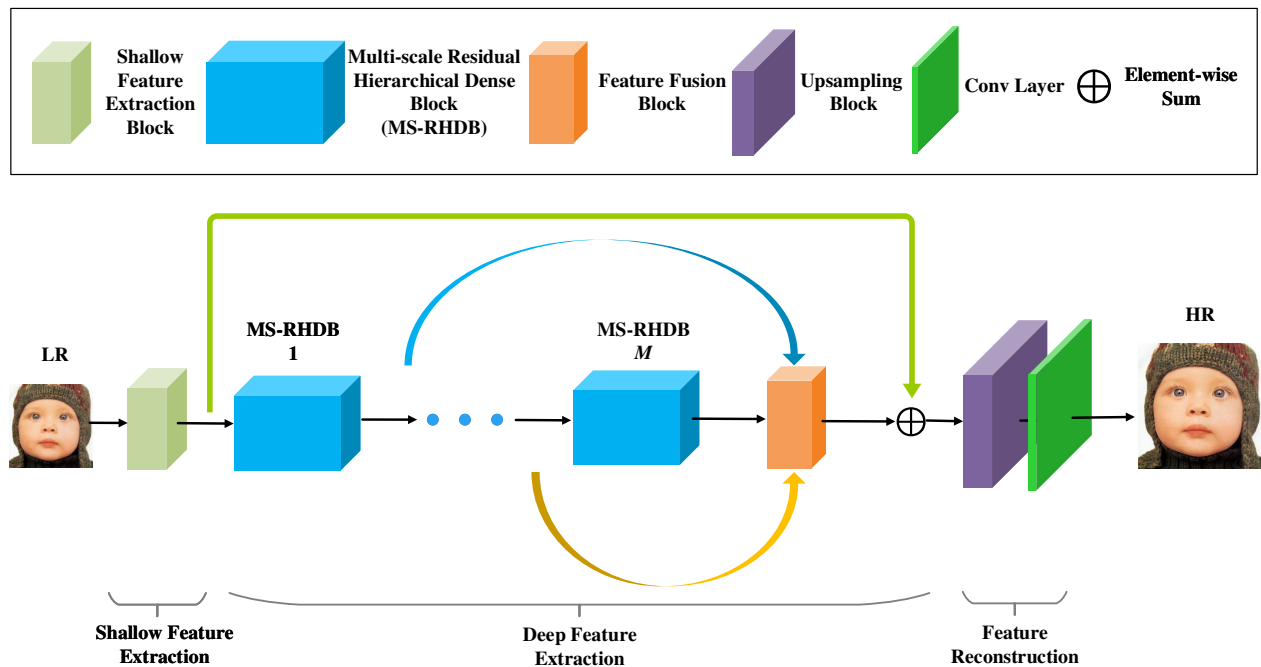


**FIGURE 1.** The main architecture of our proposed multi-scale residual hierarchical dense network (MS-RHDN). The blue and yellow arrows denote dense connections, while the green arrow denotes a shortcut connection. The MS-RHDB component is detailed below.

extract features from original LR images and then upscale the spatial size at the end of the network by a deconvolutional layer. Extracting features directly in LR images instead of interpolated images reduces computations greatly, which becomes a major choice of image super-resolution. LapSRN [4] progressively reconstructs super-resolved images with increasing scales of input images and its improved version MS-LapSRN [5] handles the multiple upsampling scales in one single model. Lim et al. applied a simplified ResNet [6] architecture by removing the unnecessary batch normalization layer to build a wide network EDSR [7] and a multi-scale deep one MDSR, which won the NTIRE2017 Super-Resolution Challenge [8]. Tai et al. [9] proposed recursive and residual learning based DRRN to reduce model parameters.

All these methods try to make full use of image information or features to improve performance, which include increasing the network depth, widening channels, or applying recursive learning. However, most CNN-based SISR models do not take full advantage of the multi-level information from different convolutional layers. Furthermore, these methods usually neglect to use the information from different scales. Objects in images may be similar at different scales and information from different scales may give some clues to help generate high-quality HR images.

To address this issue, we propose a novel network based on the multi-scale structure and residual hierarchical dense connection. The dense connection extracts more information from different layers. We use two levels of dense connections to detect local and global multi-level features. To extract

multi-scale features, we simply apply the residual atrous-spatial-pyramid-pooling structure to fully make use of the information from multiple scales in the LR images. For stabilizing the network and easing the training difficult, we use residual learning to detect more informative features.

Overall, the main contributions of our method are three-fold:

- We propose a unified framework multi-scale residual hierarchical dense network for image super-resolution. Our method aims at making full use of multi-scale and multi-level features in the LR input image.
- We propose a residual hierarchical dense module to focus on global and local multi-level features. We use sub-dense blocks (SDBs) to adaptively obtain the essential parts of the dense features. Skip connections are applied for efficient network training and performance improvements.
- We propose a residual multi-scale structure to detect multi-scale features, which can be readily applied to other super-resolution networks. Such multi-scale structure further improves the performance of the network. In addition, our model obtains much better SR performance than previous CNN-based methods.

The remainder of this paper is organized as follows: Section 2 introduces related work on image super-resolution. Section 3 presents the proposed method. Section 4 gives experimental results on benchmark datasets. Visual comparisons with other methods are also included. To show the effectiveness of the components in our network, Section 5 gives the network investigations. Finally, Section 6 draws



conclusions.

## II. RELATED WORK

The SISR methods can mainly be categorized into three classes: interpolation-based methods [10]–[13], reconstruction-based methods [14]–[16], and learning-based methods. The interpolation-based methods, such as bilinear interpolation and bicubic interpolation, are simple and fast, but suffer from over-smoothed textures and thus are not able to produce high-quality images. The reconstruction-based methods are flexible and usually use prior knowledge to produce high-frequency details. However, these methods are usually time-consuming and suffer from rapid degeneration of performance with the increasing upsampling factor.

The learning-based methods attempt to learn mappings from LR space to HR space directly. Freeman et al. [17] firstly used Markov random fields (MRF) to generate synthetic images, where the parameters of the model are learned from the examples. Chang et al. [18] used locally linear embedding (LLE) [19] to find the resolutions from the linear combination of nearest neighbors. ANR [20] proposed by Timofte et al. uses sparse learned dictionaries and applies the coefficients calculated from LR patches to the corresponding SR patches directly. A+ [21], an improved version of ANR, learns regressors on all training patches. There also exist SR methods based on decision trees or random forests such as [22]–[26] to address the SISR problem.

Recently, deep-learning based methods have shown great improvements in image super-resolution. Specifically, Dong et al. [1] firstly proposed a deep convolutional neural network SRCNN for the SISR problem. The depth of the network plays an important role in many vision tasks, Kim et al. proposed VDSR [2] with remarkable performance, which increased the depth of the network. To reduce the parameters and find the dependencies of different proceeding time, DRRN [9] uses recursive learning and the memory block with the deeper network. Instead of interpolating the original LR images to the desired size before putting them into the networks, FSRCNN [3] extracted features from the original LR images and used a deconvolutional layer to upscale the spatial size at the end of the network, which greatly reduced the computations. This manner is commonly used in recent SR methods. LapSRN [4] progressively reconstructs the HR image with increasing scales of input images. MS-LapSRN [5], an improved version of LapSRN, uses a multi-scale training strategy to handle the multiple upsampling scales in one single model. Shi et al. [27] proposed ESPCN, which introduces a sub-pixel convolutional layer for efficient upsampling. Lim et al. [7] proposed EDSR and a multi-scale deep MDSR, which removed the unnecessary batch normalization layer from the ResNet [6] architecture. SRMDNF [28] is proposed to handle multiple degradations by concatenating degradation maps and images as the input to the network and adaptively learn to produce high-quality images under different blur kernels of downsampling. ZSSR [29] (zero-shot super-resolution) uses an unsupervised approach to learn

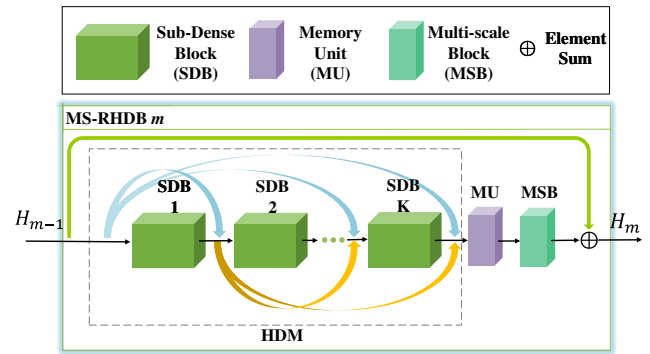


FIGURE 2. Multi-scale residual hierarchical dense block (MS-RHDB).

the mapping from LR images to HR images, whose training data are generated by downsampling the test data. D-DBPN [30] uses an error-correcting feedback mechanism for SR by iterative up and downsampling. RDN [31] proposed by Zhang et al. uses residual and dense connections and achieves state-of-the-art performance. Zhang et al. [32] proposed RNAN, where local and non-local attention blocks are used to adaptively rescale features with soft attention.

In order to produce photo-realistic SR images, Ledig et al. [33] firstly introduced residual learning and generative adversarial network (GAN) to decrease the distance between the distributions of real images and SR images. However, the images generated by SRGAN still contain noise and artifacts. Wang et al. [34] introduced an enhanced SRGAN, which applied relativistic GAN [35] to the discriminator and adopted residual scaling [36], smaller initialization, and network interpolation, to remove artifacts and won the first place in the 2018 PIRM-SR challenge in region 3. For producing realistic SR images, many loss functions have been proposed. The perceptual loss [37] is proposed to reduce the pixel-wise distances of high-level features produced by pre-trained models, e.g. VGG19 [38]. Contextual loss [39] maintains the image statistics and approximates the KL-divergence.

Making full use of the information in the LR images is the key to produce plausible SR images. To investigate multi-scale and multi-level features, we propose a multi-scale residual hierarchical dense network to obtain results with improvements in quality and quantity. We will introduce our method in the next section.

## III. PROPOSED METHOD

In this paper, our method aims to reconstruct a high-resolution image  $I^{SR} \in R^{W_r \times H_r \times C}$  from a low-resolution image  $I^{LR} \in R^{W \times H \times C}$ , where  $W$  and  $H$  are the width and height of the LR image,  $r$  is the upscaling factor, and  $C$  is the number of channels of the color space. Fig.1 shows the main framework of our network, whose components are detailed below.

## A. NETWORK ARCHITECTURE

Our proposed multi-scale residual hierarchical dense network (MS-RHDN) consists of three main components: shallow feature extraction  $F_{SF}$ , deep feature extraction  $F_{DF}$ , and feature reconstruction  $F_{REC}$ . We use one convolutional layer to extract the shallow features  $H_0$ , including edges, corners, etc., from  $I^{LR}$ :

$$H_0 = F_{SF}(I^{LR}), \quad (1)$$

where  $H_0$  is the input to the deep feature extraction module. In deep feature extraction, we use  $M$  sequential multi-scale residual hierarchical dense blocks (MS-RHDB) and a global fusion layer  $F_{GF}$  to extract and fuse multi-scale and multi-level features. Furthermore, a global skip connection is introduced to make the main parts of the network focus on high-frequency information. Formally, we have

$$\begin{aligned} H_{DF} &= F_{DF}(H_0) \\ &= H_0 + F_{GF}([H_1, H_2, \dots, H_m, \dots, H_M]) \quad (2) \\ \text{with } H_m &= F_{MSD}^m(H_{m-1}), \end{aligned}$$

where  $F_{MSD}^m$  denotes the mapping of the  $m$ -th MS-RHDB;  $[\cdot]$  stands for the concatenation operator. Finally, the feature reconstruction module produces a high-resolution image  $I^{SR}$  based on the feature  $H_{DF}$ :

$$I^{SR} = F_{REC}(H_{DF}) = F_{conv}(F_{up}(H_{DF})). \quad (3)$$

Here the feature reconstruction module is composed of an upscaling layer  $F_{up}$  and a convolutional layer  $F_{conv}$ . There have been a number of advanced upsampling structures, *e.g.*, deconvolutional layer, sub-pixel convolution, EUSR [40]. Here we adopt the sub-pixel convolution, which has been shown effective in previous works such as EDSR [7] and RDN [31].

To define a proper loss function, researchers have designed different loss functions such as  $L_2$ ,  $L_1$ , perceptual, and adversarial losses. In our work, we choose  $L_1$  loss in order to reduce computational complexity. Given a training set  $\{I_i^{LR}, I_i^{HR}\}_{i=1}^N$ , where  $I^{LR}$  is obtained by down-sampling from  $I^{HR}$  with scaling factor  $r$ , the  $L_1$  loss is defined as:

$$\begin{aligned} L_1(I_i^{SR}, I_i^{HR}) &= \frac{1}{W \times H \times C} \\ &\times \sum_{c=1}^C \sum_{w=1}^W \sum_{h=1}^H \|F_{\theta}(I_i^{LR})(w, h, c) - I_i^{HR}(w, h, c)\|_1, \quad (4) \end{aligned}$$

where  $W$ ,  $H$ , and  $C$  stand for the width, height, and channels of the low-resolution image respectively and  $r$  is the scaling factor.  $F_{\theta}$  denotes the function of our network and  $\theta$  stands for the set of parameters, which are updated by stochastic gradient descent.

## B. MULTI-SCALE RESIDUAL HIERARCHICAL DENSE BLOCK (MS-RHDB)

The proposed MS-RHDB framework mainly contains three components: a hierarchical dense module, a memory unit, and a multi-scale block. This section details the hierarchical

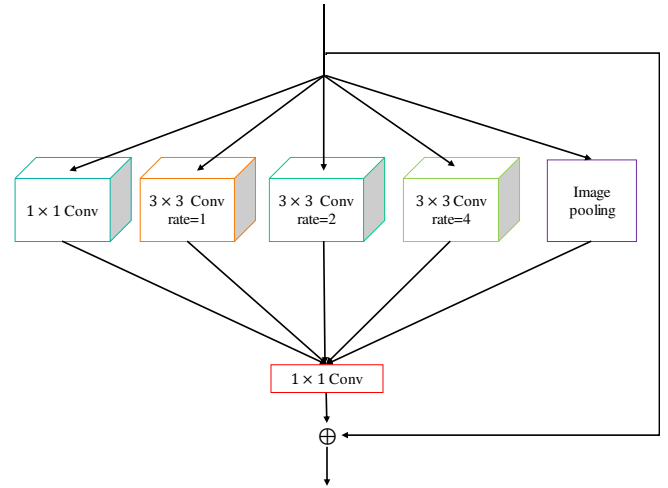


FIGURE 3. Residual multi-scale block (MSB) architecture.

dense module and the memory unit. Detailed description of the multi-scale block is given in Section III-C.

**Hierarchical dense module (HDM)** The hierarchical dense module is built to adequately exploit multi-level features. In the module,  $K$  sub-dense blocks (SDB) are arranged in a dense manner. Detailed description of SDB is introduced in Section III-D. In general, an HDM takes  $H_{m-1}$  as input, and outputs an intermediate feature  $H_m^{HDM}$ . Formally, this procedure is described as:

$$\begin{aligned} H_m^{HDM} &= F_{HDM}^m(H_{m-1}) \\ &= F_{SDB}^K([H_{m-1}, S_1, \dots, S_k, \dots, S_{K-1}]), \quad (5) \end{aligned}$$

where  $F_{HDM}^m$  denotes the function of an HDM in the  $m$ -th MS-RHDB block; and  $F_{SDB}^K$  denotes the function of the  $K$ -th SDB that constitutes  $F_{HDM}^m$ .  $S_k$  denotes the output of the  $k$ -th SDB, whose input is the concatenation of outputs of the previous  $k-1$  SDBs. Formally,  $S_k$  can be presented as:

$$S_k = F_{SDB}^k([H_{m-1}, S_1, \dots, S_{k-1}]), \quad (6)$$

where  $F_{SDB}^k$  denotes the function of the  $k$ -th SDB.  $S_k$  contains  $G$  feature-maps, where  $G$  is the number of channels and also known as growth rate in [41].

**Memory unit.** After extracting multi-level features with a set of SDBs, we use a memory unit [42] to integrate these features, which is supposed to adaptively extract unified information. Furthermore, a memory unit is also useful to reduce the number of feature-maps, thus reducing the number of parameters and computations. Specifically, the memory unit is defined as:

$$H_m^{MU} = F_{MU}^m([H_{m-1}, S_1, \dots, S_k, \dots, S_K]), \quad (7)$$

where  $F_{MU}^m$  denotes the mapping function of the memory unit in the  $m$ -th MS-RHDB; and  $H_m^{MU}$  is the output of  $F_{MU}^m$ . Following [9] [31], the memory unit is represented with a  $1 \times 1$  convolutional layer. Finally, we use a multi-scale structure, which will be introduced in section III-C, to extract

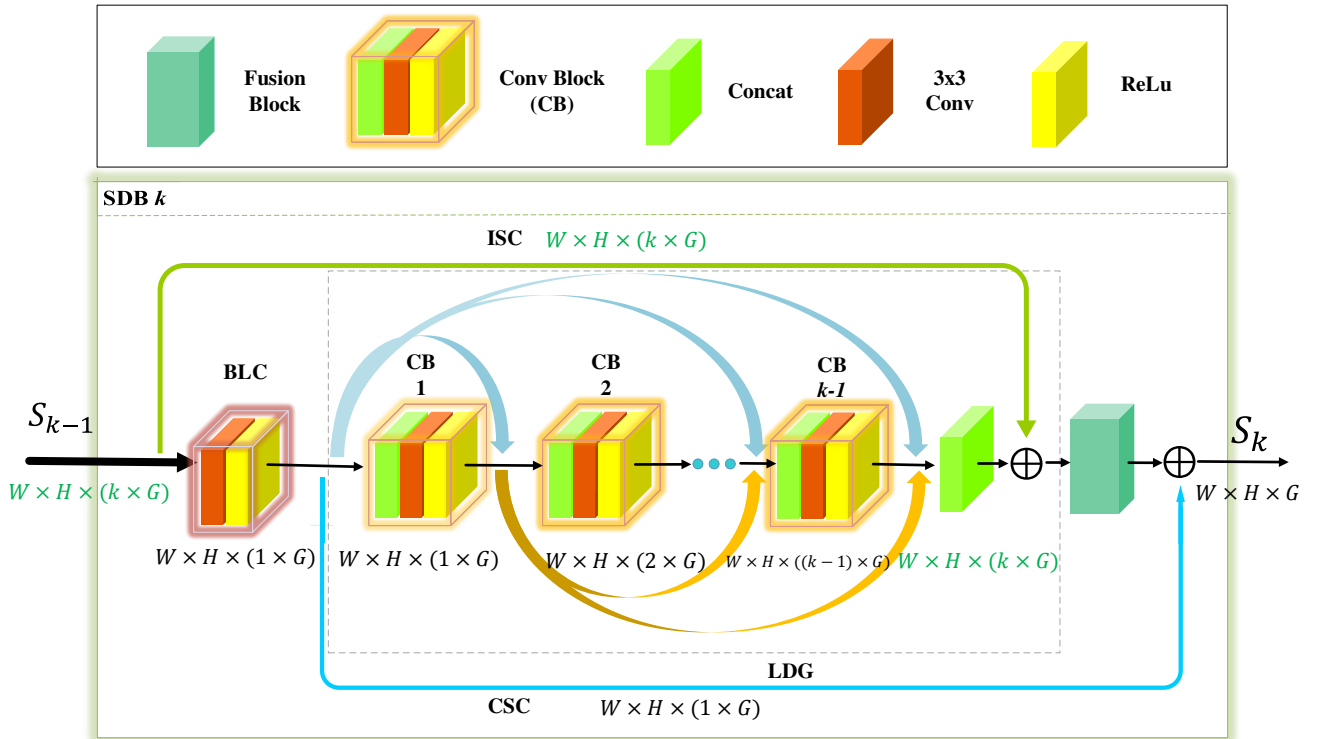


**FIGURE 4.** Network architecture of our proposed sub-dense block (SDB). For a SDB,  $W \times H \times (e \times G)$  is the input size of every Conv block (CB), and  $e$  denotes the index of the CB. The output size of each CB is  $W \times H \times (1 \times G)$ . “Concat” stands for the concatenation operator, and “3 × 3 Conv” refers to a convolutional layer with the kernel size of 3 × 3.

features from different scales for taking full advantage of fused features by the memory unit. A skip connection is introduced for a similar purpose to the global skip connection. The final output of the  $m$ -th MS-RHDB is obtained by:

$$H_m = H_{m-1} + F_{MS}^m(H_m^{MU}), \quad (8)$$

where  $F_{MS}^m$  denotes the function of the multi-scale block in the  $m$ -th MS-RHDB.

### C. MULTI-SCALE BLOCK (MSB)

As discussed above, multi-scale information is useful in generating high-quality super-resolution images. In this section, we elaborate on our multi-scale block used in (8). As shown in Fig.3, the MSB mainly consists of an atrous-spatial-pyramid-pooling (ASPP) structure and a local skip connection.

The ASPP structure is firstly introduced in DeepLabV3 [43] for handling different sizes of objects in street-scene segmentation. ASPP consists of several parallel atrous convolutional layers with different dilated rates. In our model, we apply ASPP to detect useful components of the fused hierarchical dense features. In addition, to make the network efficient and stable, we add a local skip connection to each ASPP. Formally, our multi-scale block is defined as:

$$H_m^{MS} = H_m^{MU} + F_{ASPP}^m(H_m^{MU}), \quad (9)$$

where  $F_{ASPP}^m$  denotes the function of the ASPP structure in the  $m$ -th MS-RHDB; and  $H_m^{MS}$  denotes the output of the  $m$ -th MSB.

### D. SUB-DENSE BLOCK (SDB)

In order to extract local multi-level features, we introduce a sub-dense neural network. As introduced above, an HDM is constructed by stacking several SDBs in a dense manner, where SDBs are used to extract local multi-level features from previous concatenated features. Because the input channels of each SDB may be different, the number of convolutional layers is determined by the number of the input feature-maps. More feature-maps need more layers. As shown in Fig.4, SDB contains four components: bottleneck-like compression (BLC), local dense group (LDG), input shortcut connection (ISC), and compression shortcut connection (CSC).

Firstly, we use a BLC, which is a bottleneck-like method by a  $3 \times 3$  Conv layer for reducing parameters and computations. After compressing the number of feature-maps into  $G$ , we stack several conv blocks in a manner similar to the DenseNet [41], until the number of feature-maps equals that of the input in LDG. A conv block consists of a concatenation operator applied to all the previous features, a convolutional layer with kernel size of  $3 \times 3$ , and an activation layer, as shown in Fig.4. The input of the  $k$ -th SDB,  $S_k$ , is the concatenation of the outputs of the previous  $k - 1$  layers and

**TABLE 1.** Quantitative results with the BI degradation model. The best and second best results are **highlighted** and underlined respectively.

Method	Scale	Set5		Set14		B100		Urban100		Manga109	
		PSNR	SSIM	PSNR	SSIM	PSNR	SSIM	PSNR	SSIM	PSNR	SSIM
Bicubic	×2	33.66	0.9299	30.24	0.8688	29.56	0.8431	26.88	0.8403	30.80	0.9339
SRCNN [1]	×2	36.66	0.9542	32.45	0.9067	31.36	0.8879	29.50	0.8946	35.60	0.9663
FSRCNN [3]	×2	37.05	0.9560	32.66	0.9090	31.53	0.8920	29.88	0.9020	36.67	0.9710
VDSR [2]	×2	37.53	0.9590	33.05	0.9130	31.90	0.8960	30.77	0.9140	37.22	0.9750
LapSRN [4]	×2	37.52	0.9591	33.08	0.9130	31.08	0.8950	30.41	0.9101	37.27	0.9740
MemNet [42]	×2	37.78	0.9597	33.28	0.9142	32.08	0.8978	31.31	0.9195	37.72	0.9740
EDSR [7]	×2	38.11	0.9602	<u>33.92</u>	0.9195	32.32	0.9013	32.93	0.9351	39.10	0.9773
SRMDNF [28]	×2	37.79	0.9601	33.32	0.9159	32.05	0.8985	31.33	0.9204	38.07	0.9761
D-DBPN [30]	×2	38.09	0.9600	33.85	0.9190	32.27	0.9000	32.55	0.9324	38.89	0.9775
RDN [31]	×2	38.24	0.9614	<b>34.01</b>	<b>0.9212</b>	32.34	0.9017	32.89	0.9353	39.18	0.9780
RNAN [32]	×2	38.17	0.9611	33.87	0.9207	32.32	0.9014	32.73	0.9340	39.23	0.9785
SDNND [44]	×2	38.07	0.9610	33.77	0.9195	32.25	0.9026	32.55	0.9332	—	—
MS-RHDN (ours)	×2	<u>38.26</u>	<u>0.9615</u>	<u>33.92</u>	<u>0.9206</u>	<u>32.36</u>	<u>0.9020</u>	<u>33.02</u>	<u>0.9367</u>	<u>39.33</u>	<u>0.9781</u>
MS-RHDN+ (ours)	×2	<b>38.31</b>	<b>0.9617</b>	<b>34.01</b>	<b>0.9212</b>	<b>32.40</b>	<b>0.9025</b>	<b>33.24</b>	<b>0.9382</b>	<b>39.50</b>	<b>0.9785</b>
Bicubic	×3	30.39	0.8682	27.55	0.7742	27.21	0.7385	24.46	0.7349	26.95	0.8556
SRCNN [1]	×3	32.75	0.9090	29.30	0.8215	28.41	0.7863	26.24	0.7989	30.48	0.9117
FSRCNN [3]	×3	33.18	0.9140	29.37	0.8240	28.53	0.7910	26.43	0.8080	31.10	0.9210
VDSR [2]	×3	33.67	0.9210	29.78	0.8320	28.83	0.7990	27.14	0.8290	32.01	0.9340
LapSRN [4]	×3	33.82	0.9227	29.87	0.8320	28.82	0.7980	27.07	0.8280	32.21	0.9350
MemNet [42]	×3	34.09	0.9248	30.00	0.8350	28.96	0.8001	27.56	0.8376	32.51	0.9369
EDSR [7]	×3	34.65	0.9280	30.52	0.8462	29.25	0.8093	28.80	0.8653	34.17	0.9476
SRMDNF [28]	×3	34.12	0.9254	30.04	0.8382	28.97	0.8025	27.57	0.8398	33.00	0.9403
RDN [31]	×3	34.71	0.9296	30.57	0.8468	29.26	0.8093	28.80	0.8653	34.13	0.9484
SDNND [44]	×3	34.41	0.9277	30.25	0.8425	29.10	0.8076	28.35	0.8571	—	—
MS-RHDN (ours)	×3	<u>34.76</u>	<u>0.9302</u>	<u>30.61</u>	<u>0.8475</u>	<u>29.29</u>	<u>0.8104</u>	<u>28.95</u>	<u>0.8681</u>	<u>34.40</u>	<u>0.9497</u>
MS-RHDN+ (ours)	×3	<b>34.82</b>	<b>0.9305</b>	<b>30.71</b>	<b>0.8490</b>	<b>29.34</b>	<b>0.8114</b>	<b>29.16</b>	<b>0.8712</b>	<b>34.69</b>	<b>0.9510</b>
Bicubic	×4	28.42	0.8104	26.00	0.7027	25.96	0.6675	23.14	0.6577	24.89	0.7866
SRCNN [1]	×4	30.48	0.8628	27.50	0.7513	26.90	0.7101	24.52	0.7221	27.58	0.8555
FSRCNN [3]	×4	30.72	0.8660	27.61	0.7550	26.98	0.7150	24.62	0.7280	27.90	0.8610
VDSR [2]	×4	31.35	0.8830	28.02	0.7680	27.29	0.7260	25.18	0.7540	28.83	0.8870
LapSRN [4]	×4	31.54	0.8850	28.19	0.7720	27.32	0.7270	25.21	0.7551	29.09	0.8900
MemNet [42]	×4	31.74	0.8893	28.26	0.7723	27.40	0.7281	25.50	0.7630	29.42	0.8942
EDSR [7]	×4	32.46	0.8968	28.80	0.7876	27.71	0.7420	26.64	0.8033	31.02	0.9148
SRMDNF [28]	×4	31.96	0.8925	28.35	0.7787	27.49	0.7337	25.68	0.7731	30.09	0.9024
D-DBPN [30]	×4	32.47	0.8980	28.82	0.7860	27.72	0.7400	26.38	0.7946	30.91	0.9137
RDN [31]	×4	32.47	0.8990	28.81	0.7871	27.72	0.7419	26.61	0.8028	31.00	0.9151
RNAN [32]	×4	32.49	0.8982	28.83	0.7878	27.72	0.7421	26.61	0.8023	31.09	0.9149
SDNND [44]	×4	32.21	0.8954	28.54	0.7817	27.55	0.7364	26.23	0.7914	—	—
MS-RHDN (ours)	×4	<u>32.62</u>	<u>0.8998</u>	<u>28.85</u>	<u>0.7881</u>	<u>27.75</u>	<u>0.7424</u>	<u>26.72</u>	<u>0.8059</u>	<u>31.30</u>	<u>0.9179</u>
MS-RHDN+ (ours)	×4	<b>32.70</b>	<b>0.9009</b>	<b>28.97</b>	<b>0.7901</b>	<b>27.81</b>	<b>0.7438</b>	<b>26.92</b>	<b>0.8101</b>	<b>31.62</b>	<b>0.9205</b>
Bicubic	×8	24.40	0.6580	23.10	0.5660	23.67	0.5480	20.74	0.5160	21.47	0.6500
SRCNN [1]	×8	25.33	0.6900	23.76	0.5910	24.13	0.5660	21.29	0.5440	22.46	0.6950
FSRCNN [3]	×8	20.13	0.5520	19.75	0.4820	24.21	0.5680	21.32	0.5380	22.39	0.6730
SCN [45]	×8	25.59	0.7071	24.02	0.6028	24.30	0.5698	21.52	0.5571	22.68	0.6963
VDSR [2]	×8	25.93	0.7240	24.26	0.6140	24.49	0.5830	21.70	0.5710	23.16	0.7250
LapSRN [4]	×8	26.15	0.7380	24.35	0.6200	24.54	0.5860	21.81	0.5810	23.39	0.7350
MemNet [42]	×8	26.16	0.7414	24.38	0.6199	24.58	0.5842	21.89	0.5825	23.56	0.7387
MS-LapSRN [5]	×8	26.34	0.7558	24.57	0.6273	24.65	0.5895	22.06	0.5963	23.90	0.7564
EDSR [7]	×8	26.96	0.7762	24.91	0.6420	24.81	0.5985	22.51	0.6221	24.69	0.7841
D-DBPN [30]	×8	<u>27.21</u>	<u>0.7840</u>	<u>25.13</u>	<u>0.6480</u>	24.88	0.6010	22.73	0.6312	<u>25.14</u>	<b>0.7987</b>
MS-RHDN (ours)	×8	27.13	0.7820	<u>25.13</u>	0.6471	<u>24.89</u>	<u>0.6016</u>	<u>22.76</u>	<u>0.6326</u>	24.94	0.7907
MS-RHDN+ (ours)	×8	<b>27.32</b>	<b>0.7876</b>	<b>25.27</b>	<b>0.6505</b>	<b>24.96</b>	<b>0.6037</b>	<b>22.93</b>	<b>0.6388</b>	<b>25.21</b>	<u>0.7971</u>

$H_{m-1}$ , which contains  $k \times G$  channels. As a result, the LDG in the  $k$ -th SDB requires  $k - 1$  convolutional layers to reach the same number of channels as that of the input. Formally, the LDG is described as:

$$S_k^{\text{LDG}} = F_{\text{LDG}}^k([S_{k-1}^{\text{BLC}}, S_{k-1,1}, \dots, S_{k-1,d}, \dots, S_{k-1,k-1}]), \quad (10)$$

where  $S_{k-1}^{\text{BLC}}$  is the output of BLC, and  $S_{k-1,d}$  is the output of the  $d$ -th Conv in the  $k$ -th SDB.  $F_{\text{LDG}}^k$  denotes the function of the local dense group in the  $k$ -th SDB and  $S_k^{\text{LDG}}$  is its output. Similarly, the input of the  $d$ -th Conv is the concatenation of proceeding layers. In SDB, the local dense group adaptively detects local multi-level features according to the amount of

information that the input has.

**ISC and CSC.** At the same time, the ISC stands for an element-wise addition in the input  $S_{k-1}$  and the multi-level features  $S_{k-1,k-1}$ . After that, we apply a  $1 \times 1$  Conv to fuse the number of feature-maps into  $G$ . Finally, the compressed feature  $S_{k-1}^{\text{BLC}}$  is added to the output of the fusion block by CSC. These two shortcut connections are important for detecting more informative cues and improving performance, as well as stabilizing the network.

## E. IMPLEMENTATION DETAILS

In this section, we specify some implementation details of our proposed MS-RHDN. We set the kernel size of all the



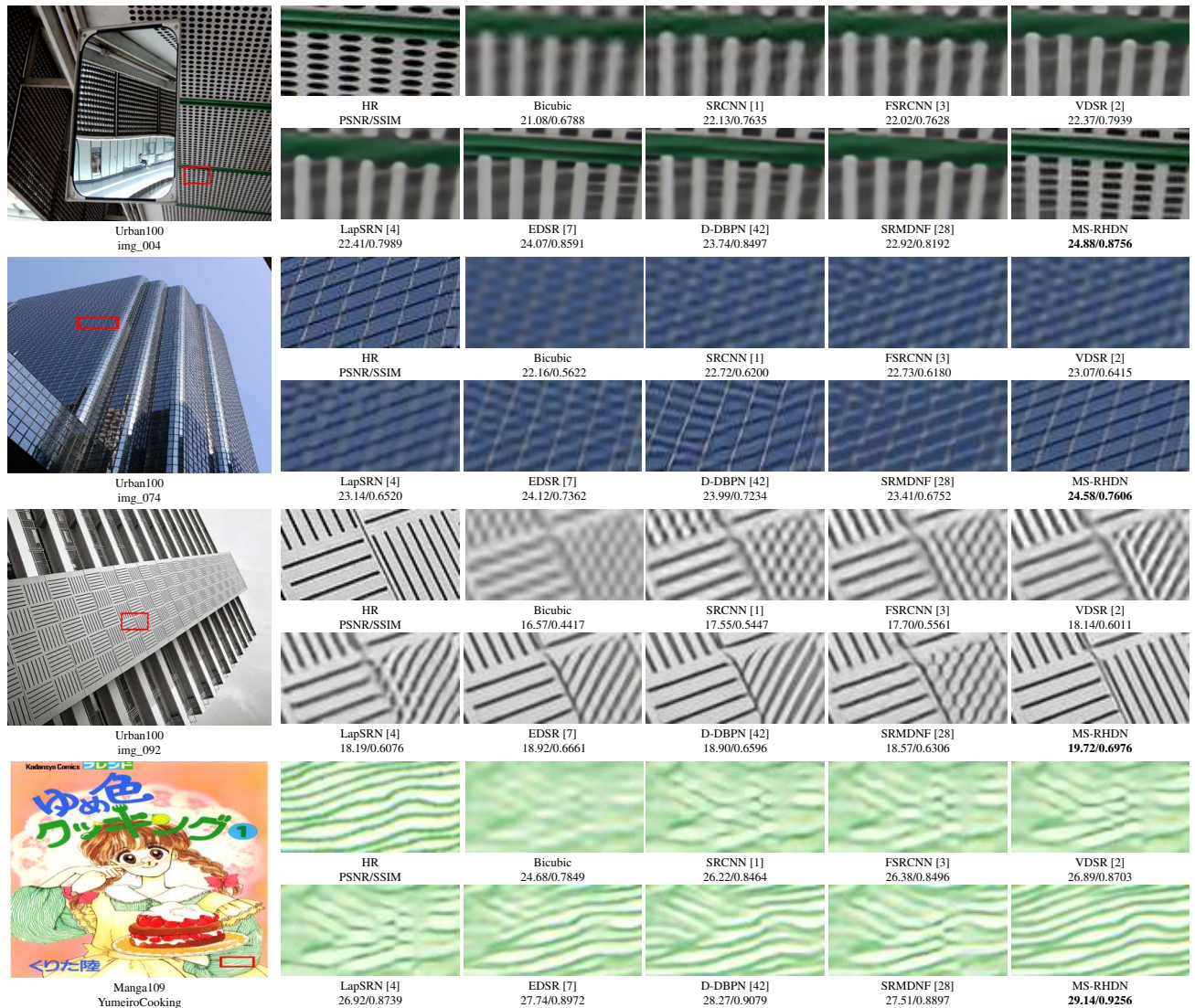


FIGURE 5. Visual comparison for  $4 \times$  SR with the BI model on the Urban100 and Manga109 datasets. The best results are highlighted.

convolutional layers to  $3 \times 3$ , except for the fusion layers, whose kernel sizes are set to  $1 \times 1$ . The number of MS-RHDB is set to  $M = 10$ . In each MS-RHDB, we set the number of SDBs as  $K = 5$ . The number of convolutional layers in LDG is decided adaptively, depending on the input. As an illustration, the LDG in the  $k$ -th SDB stack  $k - 1$  convolutional layers organized in a dense manner to get the same number of channels as the input. We set the growth rate as  $G = 64$ . We use ESPCN [27] to upscale the coarse resolution feature-maps to fine ones in our reconstruction module. At the tail of the network, we use 3 convolutional filters to generate high-quality super-resolved images with 3 color channels.

**Difference to RDN.** Here, we mainly summarize three differences between our method and the RDN [31]. First, both RDN and our model use dense connections. However, multi-level dense connections are adopted in our MS-RHDN, compared to one level in RDN. Second, we apply multi-

scale blocks to our MS-RHDN, which aims at extracting multi-scale information from features, while RDN ignores this important information. Third, we proposed SDBs to learn local hierarchical features instead of simple convolutional layers in RDN. Experiments in the next section show that our MS-RHDN outperforms RDN in benchmark datasets with less parameters.

#### IV. EXPERIMENTAL RESULTS

In this section, we conduct quantitative and visual comparisons with several state-of-the-art methods on benchmark datasets under two commonly used image degradations: bicubic downsampling and blur-downsampling, respectively.

##### A. SETTINGS

We use the DIV2K dataset [8] as our training set, which contains 800, 100 and 100 images of 2K-resolution for training, validation, and testing, respectively. The LR images



**TABLE 2.** Quantitative results with the blur-down degradation model. Best and second best results are **highlighted** and underlined.

Method	Scale	Set5		Set14		B100		Urban100		Manga109	
		PSNR	SSIM	PSNR	SSIM	PSNR	SSIM	PSNR	SSIM	PSNR	SSIM
Bicubic	$\times 3$	28.78	0.8308	26.38	0.7271	26.33	0.6918	23.52	0.6862	25.46	0.8149
SPMSR [46]	$\times 3$	32.21	0.9001	28.89	0.8105	28.13	0.7740	25.84	0.7856	29.64	0.9003
SRCNN [1]	$\times 3$	32.05	0.8944	28.80	0.8074	28.13	0.7736	25.70	0.7770	29.47	0.8924
FSRCNN [3]	$\times 3$	26.23	0.8124	24.44	0.7106	24.86	0.6832	22.04	0.6745	23.04	0.7927
VDSR [2]	$\times 3$	33.25	0.9150	29.46	0.8244	28.57	0.7893	26.61	0.8136	31.06	0.9234
IRCNN [47]	$\times 3$	33.38	0.9182	29.63	0.8281	28.65	0.7922	26.77	0.8154	31.15	0.9245
RDN [31]	$\times 3$	34.58	0.9280	30.53	0.8447	29.23	0.8079	28.46	0.8582	33.97	0.9465
MS-RHDN (ours)	$\times 3$	<u>34.76</u>	<u>0.9292</u>	<u>30.67</u>	<u>0.8468</u>	<u>29.32</u>	<u>0.8098</u>	<u>28.83</u>	<u>0.8648</u>	<u>34.49</u>	<u>0.9491</u>
MS-RHDN+ (ours)	$\times 3$	<b>34.82</b>	<b>0.9298</b>	<b>30.75</b>	<b>0.8481</b>	<b>29.32</b>	<b>0.8108</b>	<b>29.04</b>	<b>0.8679</b>	<b>34.78</b>	<b>0.9505</b>

are obtained by bicubic downsampling (BI) from the source high-resolution images. At testing, we use five standard benchmark datasets: Set5 [48], Set14 [49], BSD100 [50], Urban100 [51], and Manga109 [52]. We transform the images into YCrCb color space and evaluate the performance by PSNR and SSIM on the Y channel.

In training, images are augmented by rotating and flipping. The batch size is set to 16. Our MS-RHDN is trained based on image patches and optimized with the ADAM optimizer [53]. The hyperparameters  $\beta_1$  and  $\beta_2$  in the ADAM optimizers are set to  $\beta_1 = 0.9$  and  $\beta_2 = 0.999$ . We randomly crop  $48 \times 48$  patches from LR images as the input of the network. Following [4], [7], [27], [31], [32], the initial learning rate is set to  $1 \times 10^{-4}$ , which decays to half every  $2 \times 10^5$  iterations. We implement our model using the Pytorch [54] framework with a Titan Xp GPU. Training the MS-RHDN roughly takes one day with  $2 \times 10^5$  iterations.

## B. COMPARISONS WITH STATE-OF-THE-ART METHODS

We compare our model with 13 state-of-the-art image SR algorithms: SRCNN [1], VDSR [2], FSRCNN [3], SCN [45], LapSRN [4], MemNet [42], EDSR [7], SRMDNF [28], D-DBPN [30], RDN [28], RNAN [32], and SDNND [44]. Similar to [7], [31], [55], we also apply a self-ensemble strategy, which rotates and flips inputs to generate different versions of high-resolution images. The corresponding inverse transforms are applied to generate an HR image, which is an average version of all the HR images. This version is denoted as the self-ensembled MS-RHDN or MS-RHDN+.

**Quantitative comparison.** Table 1 shows the results of the proposed method and state-of-the-art methods for  $\times 2$ ,  $\times 3$ ,  $\times 4$ , and  $\times 8$  SR. We directly adopt the results of RNAN [32] and SDNND [44]. It can be seen that our MS-RHDN+ performs the best on all the test datasets in most scaling factors by a large margin. The MS-RHDN also outperforms other compared methods even without self-ensemble. This indicates that our network is effective in detecting comprehensive features for reconstructing tiny textures. Besides, our MS-RHDN obtains larger margins with the increase of scaling factors. We argue that it is more essential to make full use of information in LR images for a large scaling factor. The observations demonstrate that the multi-scale block and residual hierarchical dense structure allow our network to further extract more informative features and improve the

performance.

**Qualitative comparison.** Next, we qualitatively compare our method with state-of-the-art methods. Fig.5 shows the visual comparisons of SR images generated by our method and the methods compared. We obtain several observations from Fig.5. For image ‘img\_004’ in Urban100, most compared methods produce images with blurring artifacts. What is worse, most of them cannot recover the detailed textures of the green horizontal line and lattices. However, our method can generate more tiny textures and remove the artifacts. For image ‘img\_074’, we can find that most compared methods cannot generate the horizontal line correctly and also suffer from blurring artifacts. Some of them even produce edges with wrong directions. By contrast, our MS-RHDN shows great abilities in producing accurate information from the LR image. For image ‘img\_092’, we observe that Bicubic, SRCNN, FSRCNN, VDSR, and LapSRN suffer from blurring artifacts. Even though EDSR, D-DBPN, and SRMDNF can recover some high-frequency information, the right part of the cropped image generated by these methods shows wrong directions of the gap with over-smoothed edges. Our MS-RHDN can be more faithful to the ground truth. For image ‘YumeiroCooking’, due to the abundance of textures, most compared methods cannot fully recover them and obviously produce blurring artifacts. Our method achieves a better result, which is more similar to the HR image.

Overall, our method shows better performance both quantitatively and visually, as it provides a nice way to make full use of features in LR images. Our proposed residual hierarchical dense module successfully detects multi-level features. The multi-scale block is further used to extract information from multiple scales. Multiple residual connections are applied to make the network focus on important parts, and to facilitate the training of the proposed network.

Following [31], [47], we further apply our method to recover images from a blur-down degradation model. A high-resolution image is first blurred by a Gaussian kernel, and then downsampled with a scaling factor. The size of the Gaussian kernel is  $7 \times 7$  with standard deviation of 1.6. We compare our method with 6 state-of-the-art methods: SPMSR [46], SRCNN [1], FSRCNN [3], VDSR [2], IRCNN [47], and RDN [31]. Table 2 shows the results of our method and the compared methods in terms of PSNR and SSIM. We observe that our MS-RHDN has much better

FIGURE 6. Visual comparison for  $3\times$  SR with the BD model. The best results are highlighted.TABLE 3. Investigations of HDM (including ISC, CSC, LDG) and MSB. We observe the best PSNR (dB) values on Set5 ( $4\times$ ) in 100 epochs.

Structure		1	2	3	4	5	6	7	8	9
Hierarchical Dense Module (HDM)	LDG	×	×	✓	✓	✓	✓	✓	✓	✓
	ISC	×	×	×	✓	×	✓	✓	×	✓
	CSC	×	×	×	×	✓	✓	×	✓	✓
Multi-Scale Block (MSB)		×	✓	×	×	×	×	✓	✓	✓
PSNR on Set5 ( $4\times$ )		31.50	31.94	31.82	31.87	31.87	31.93	32.01	31.97	32.05

performance on all the benchmark datasets, and MS-RHDN+ achieves the best results. Our methods outperform RDN by a large margin. The observations indicate that the structure MS-RHDN is more efficient and has a stronger ability to recover images from the blur-down degradation model. Fig. 6 demonstrates visual comparisons for  $3\times$  SR under the blur-down degradation model. For image ‘img\_046’ in Urban100, it is observed that the two patches generated by Bicubic are totally blurred and lose most details. RDN can recover some details but produces some edges with wrong directions. In contrast, MS-RHDN obtains much better performance with sharper edges and correct structures. However, it can be seen from the left parts of the cropped patches on the first line of Fig. 6 that it is challenging for our method and the RDN to recover tiny textures, as these textures are badly blurred in the input LR image. This problem is also the concern in other single image super-resolution methods. Nevertheless, if we zoom in the picture, we can find that our method can still generate edge effect even in the left part of the cropped patch, while the RDN cannot. For image ‘MisutenaideDaisy’ in

Manga109, characters in the two patches produced by Bicubic cannot even be recognized by eyeballing. RDN recovers some details of the characters with simple structures, *e.g.*, “c” and “s”. However, some characters in the first patch suffer from blurring artifacts and lose some structures. In comparison, MS-RHDN can recover more details and maintain the right structures. In the second patch, RDN generates characters with over-smoothed edges and blurring artifacts. In contrast, our MS-RHDN alleviates the over-smoothness and blurring-artifacts issues by recovering sharper edges. It also demonstrates the promising potential to make full use of the multi-level and multi-scale features for SR with a blur-down degradation model.

## V. NETWORK INVESTIGATIONS

We show ablation investigations on the hierarchical dense module and the multi-scale block in table 3. The structure 9 has 10 MS-RHDBs ( $M=10$ ), 5 SDBs ( $K=5$ ), and growth rate ( $G=32$ ). We set the batch size to 8 for fast training. To show the superiority of our structure and reduce the influence

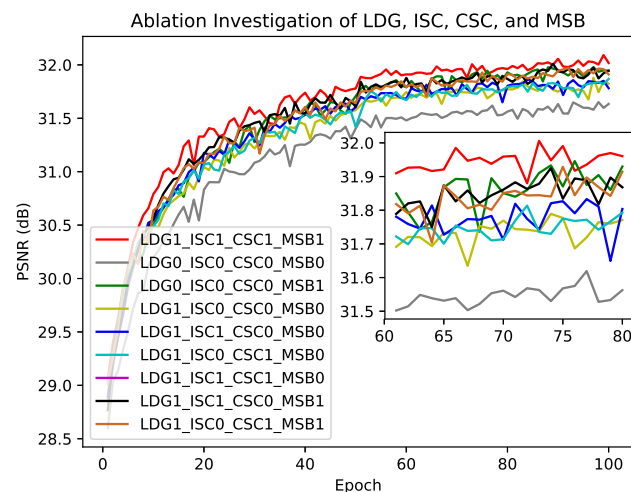


FIGURE 7. Visualisation of the convergence rates using combinations of LDG, ISC, CSC, and MSB. The curves for each combination are based on the PSNR calculated for Set5 with scaling factor  $\times 4$  over 100 epochs.

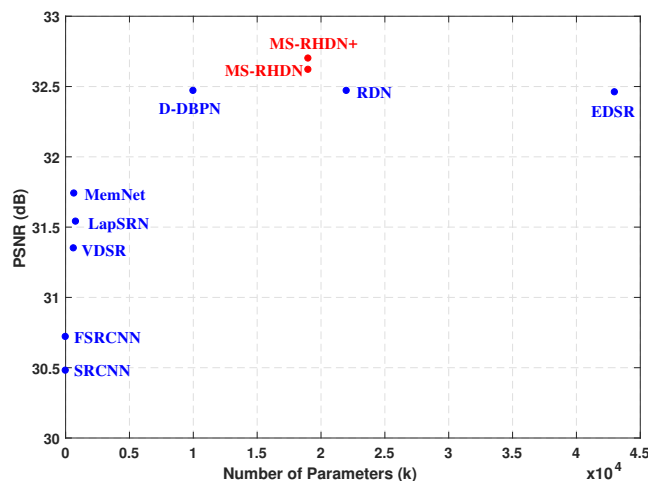


FIGURE 8. Comparison of our method and the state-of-the-art models on Set5 ( $\times 4$ ) with respect to PSNR and the number of parameters.

of parameters, we design another 8 network structures with approximate parameters by varying the numbers of MS-RHDB and SDB.

**Hierarchical dense module (HDM).** To demonstrate the effect of our HDM, we add in different configurations with LDG, ISC, or/and CSC. In table 3, when LDG, ISC, and CSC are absent, the PSNR value on Set5 is relatively low. The positive effect of LDG is demonstrated by the performance improvement from structure 1 to 3. Similarly, ISC and CSC are significant for producing high-quality images. The performance increases with LDG, ISC, or CSC, and we can obtain improvements by using all of them. After adding HDMs, the performance increases to 31.93 dB compared to the structure 1 with 31.50 dB. This demonstrates the efficiency of our HDM in extracting informative features.

**Multi-scale block.** Finally, we show the effect of the multi-scale block based on the observations from Table 3.

When MSBs are added, the PSNR value increases from 31.93 dB in structure 6 to 32.05 dB in structure 9. Comparisons between structure 1 and 2 or structure 4 and 7 demonstrate the effectiveness of the MSB as well. The performance improvements obtained by the MSB indicate that the multi-scale features have played an important part in generating SR images.

In Fig.7, we further visualize the training process of these nine structures on the PSNR of Set5 ( $\times 4$ ). We can observe that the curves are consistent with our analyses, and the LDG, ISC, CSC, and MSB can further improve the performance. These quantitative and visual analyses show the superiority and effectiveness of our proposed LDG, ISC, CSC, and MSB elements.

Fig.8 shows comparisons of PSNR versus the number of parameters of our method and the compared methods. We can observe that our MS-RHDN and MS-RHDN+ have only half number of parameters of EDSR [7] and also fewer parameters than RDN [31]. They also achieve better performance. It demonstrates that our model has a more effective structure and a better trade-off between performance and model size.

## VI. CONCLUSIONS

In this paper, we propose a novel multi-scale residual hierarchical dense network for high-quality image super-resolution. Our model aims at fully utilizing features in LR images. Specifically, the residual hierarchical dense structure is used for adaptively extracting multi-level features. Meanwhile, the multi-scale block serves to obtain multi-scale features. Furthermore, residual learning mechanism is used to stabilize the training of our model, and to pay attention to more informative features. Extensive experiments on benchmark datasets illustrate the effectiveness of our MS-RHDN in image super-resolution.

## REFERENCES

- [1] C. Dong, C. C. Loy, K. He, and X. Tang, "Image super-resolution using deep convolutional networks," *IEEE Transactions on Pattern Analysis and Machine Intelligence*, vol. 38, no. 2, pp. 295–307, 2016.
- [2] J. Kim, J. K. Lee, and K. M. Lee, "Accurate image super-resolution using very deep convolutional networks," in *2016 IEEE Conference on Computer Vision and Pattern Recognition (CVPR)*, Jun. 2016, pp. 1646–1654.
- [3] C. Dong, C. C. Loy, K. He, and X. Tang, "Image super-resolution using deep convolutional networks," *IEEE Transactions on Pattern Analysis and Machine Intelligence*, vol. 38, no. 2, pp. 295–307, Feb. 2016.
- [4] W. Lai, J. Huang, N. Ahuja, and M. Yang, "Deep laplacian pyramid networks for fast and accurate super-resolution," in *2017 IEEE Conference on Computer Vision and Pattern Recognition (CVPR)*, Jul. 2017, pp. 5835–5843.
- [5] W. Lai, J. Huang, N. Ahuja, and M. Yang, "Fast and accurate image super-resolution with deep Laplacian pyramid networks," *IEEE Transactions on Pattern Analysis and Machine Intelligence*, pp. 1–14, Aug. 2018.
- [6] K. He, X. Zhang, S. Ren, and J. Sun, "Deep residual learning for image recognition," in *2016 IEEE Conference on Computer Vision and Pattern Recognition (CVPR)*, Jun. 2016, pp. 770–778.
- [7] B. Lim, S. Son, H. Kim, S. Nah, and K. M. Lee, "Enhanced deep residual networks for single image super-resolution," in *2017 IEEE Conference on Computer Vision and Pattern Recognition Workshops (CVPRW)*, Jul. 2017, pp. 1132–1140.
- [8] R. Timofte, E. Agustsson, L. V. Gool, M. Yang, L. Zhang, B. Lim, S. Son, H. Kim, S. Nah, K. M. Lee, X. Wang, Y. Tian, K. Yu, Y. Zhang, S. Wu,



- C. Dong, L. Lin, Y. Qiao, C. C. Loy, W. Bae, J. Yoo, Y. Han, J. C. Ye, J. Choi, M. Kim, Y. Fan, J. Yu, W. Han, D. Liu, H. Yu, Z. Wang, H. Shi, X. Wang, T. S. Huang, Y. Chen, K. Zhang, W. Zuo, Z. Tang, L. Luo, S. Li, M. Fu, L. Cao, W. Heng, G. Bui, T. Le, Y. Duan, D. Tao, R. Wang, X. Lin, J. Pang, J. Xu, Y. Zhao, X. Xu, J. Pan, D. Sun, Y. Zhang, X. Song, Y. Dai, X. Qin, X. Huynh, T. Guo, H. S. Mousavi, T. H. Vu, V. Monga, C. Cruz, K. Egiazarian, V. Katkovnik, R. Mehta, A. K. Jain, A. Agarwalla, C. V. S. Praveen, R. Zhou, H. Wen, C. Zhu, Z. Xia, Z. Wang, and Q. Guo, "Ntire 2017 challenge on single image super-resolution: Methods and results," in 2017 IEEE Conference on Computer Vision and Pattern Recognition Workshops (CVPRW), Jul. 2017, pp. 1110–1121.
- [9] Y. Tai, J. Yang, and X. Liu, "Image super-resolution via deep recursive residual network," in 2017 IEEE Conference on Computer Vision and Pattern Recognition (CVPR), Jul. 2017, pp. 2790–2798.
- [10] H. Hou and H. Andrews, "Cubic splines for image interpolation and digital filtering," IEEE Transactions on Acoustics, Speech, and Signal Processing, vol. 26, no. 6, pp. 508–517, Dec. 1978.
- [11] X. Li and M. T. Orchard, "New edge-directed interpolation," IEEE Transactions on Image Processing, vol. 10, no. 10, pp. 1521–1527, Oct. 2001.
- [12] L. Zhang and X. Wu, "An edge-guided image interpolation algorithm via directional filtering and data fusion," IEEE Transactions on Image Processing, vol. 15, no. 8, pp. 2226–2238, Aug. 2006.
- [13] M. Li and T. Q. Nguyen, "Markov random field model-based edge-directed image interpolation," IEEE Transactions on Image Processing, vol. 17, no. 7, pp. 1121–1128, Jul. 2008.
- [14] M. Irani and S. Peleg, "Improving resolution by image registration," CVGIP: Graphical Models and Image Processing, vol. 53, no. 3, pp. 231–239, 1991.
- [15] S. Baker and T. Kanade, "Limits on super-resolution and how to break them," IEEE Transactions on Pattern Analysis and Machine Intelligence, vol. 24, no. 9, pp. 1167–1183, Sep. 2002.
- [16] Z. Lin and H.-Y. Shum, "Fundamental limits of reconstruction-based superresolution algorithms under local translation," IEEE Transactions on Pattern Analysis and Machine Intelligence, vol. 26, no. 1, pp. 83–97, Jan. 2004.
- [17] W. T. Freeman and E. C. Pasztor, "Learning low-level vision," in Proceedings of the Seventh IEEE International Conference on Computer Vision, vol. 2, Sep. 1999, pp. 1182–1189.
- [18] H. Chang, D.-Y. Yeung, and Y. Xiong, "Super-resolution through neighbor embedding," in 2004 IEEE Computer Society Conference on Computer Vision and Pattern Recognition (CVPR), vol. 1, Jun. 2004, pp. 1–1.
- [19] S. T. Roweis and L. K. Saul, "Nonlinear dimensionality reduction by locally linear embedding," Science, vol. 290, no. 5500, pp. 2323–2326, 2000.
- [20] R. Timofte, V. De, and L. V. Gool, "Anchored neighborhood regression for fast example-based super-resolution," in 2013 IEEE International Conference on Computer Vision (ICCV), Dec. 2013, pp. 1920–1927.
- [21] R. Timofte, V. De Smet, and L. Van Gool, "A+: Adjusted anchored neighborhood regression for fast super-resolution," in Asian Conference on Computer Vision (ACCV), 2014, pp. 111–126.
- [22] J. Huang and W. Siu, "Learning hierarchical decision trees for single-image super-resolution," IEEE Transactions on Circuits and Systems for Video Technology, vol. 27, no. 5, pp. 937–950, May. 2017.
- [23] J. Huang and W. Siu, "Practical application of random forests for super-resolution imaging," in 2015 IEEE International Symposium on Circuits and Systems (ISCAS), May. 2015, pp. 2161–2164.
- [24] J. Huang, W. Siu, and T. Liu, "Fast image interpolation via random forests," IEEE Transactions on Image Processing, vol. 24, no. 10, pp. 3232–3245, Oct. 2015.
- [25] S. Schuler, C. Leistner, and H. Bischof, "Fast and accurate image upscaling with super-resolution forests," in 2015 IEEE Conference on Computer Vision and Pattern Recognition (CVPR), Jun. 2015, pp. 3791–3799.
- [26] D. Xiong, Q. Gui, W. Hou, and M. Ding, "Gradient boosting for single image super-resolution," Information Sciences, vol. 454, pp. 328–343, 2018.
- [27] W. Shi, J. Caballero, F. Huszar, J. Totz, A. P. Aitken, R. Bishop, D. Rueckert, and Z. Wang, "Real-time single image and video super-resolution using an efficient sub-pixel convolutional neural network," in 2016 IEEE Conference on Computer Vision and Pattern Recognition (CVPR), Jun. 2016, pp. 1874–1883.
- [28] K. Zhang, W. Zuo, and L. Zhang, "Learning a single convolutional super-resolution network for multiple degradations," in 2018 IEEE Conference on Computer Vision and Pattern Recognition (CVPR), Jun. 2018, pp. 3262–3271.
- [29] A. Shocher, N. Cohen, and M. Irani, "Zero-shot super-resolution using deep internal learning," in 2018 IEEE Conference on Computer Vision and Pattern Recognition (CVPR), Jun. 2018, pp. 3118–3126.
- [30] M. Haris, G. Shakhnarovich, and N. Ukita, "Deep back-projection networks for super-resolution," in 2018 IEEE Conference on Computer Vision and Pattern Recognition (CVPR), Jun. 2018, pp. 1664–1673.
- [31] Y. Zhang, Y. Tian, Y. Kong, B. Zhong, and Y. Fu, "Residual dense network for image super-resolution," in 2018 IEEE Conference on Computer Vision and Pattern Recognition (CVPR), Jun. 2018, pp. 2472–2481.
- [32] Y. Zhang, K. Li, K. Li, B. Zhong, and Y. Fu, "Residual non-local attention networks for image restoration," in International Conference on Learning Representations (ICLR), 2019.
- [33] C. Ledig, L. Theis, F. Huszar, J. Caballero, A. Cunningham, A. Acosta, A. Aitken, A. Tejani, J. Totz, Z. Wang, and W. Shi, "Photo-realistic single image super-resolution using a generative adversarial network," in 2017 IEEE Conference on Computer Vision and Pattern Recognition (CVPR), Jul. 2017, pp. 105–114.
- [34] X. Wang, K. Yu, S. Wu, J. Gu, Y. Liu, C. Dong, Y. Qiao, and C. C. Loy, "Esrnet: Enhanced super-resolution generative adversarial networks," in The European Conference on Computer Vision Workshops (ECCVW), Sep. 2018.
- [35] A. Jolicœur-Martineau, "The relativistic discriminator: a key element missing from standard GAN," arXiv preprint arXiv:1807.00734, 2018.
- [36] C. Szegedy, S. Ioffe, V. Vanhoucke, and A. A. Alemi, "Inception-v4, Inception-Resnet and the impact of residual connections on learning," in Thirty-First AAAI Conference on Artificial Intelligence, 2017.
- [37] J. Johnson, A. Alahi, and L. Fei-Fei, "Perceptual losses for real-time style transfer and super-resolution," in The European conference on computer vision (ECCV), 2016, pp. 694–711.
- [38] K. Simonyan and A. Zisserman, "Very deep convolutional networks for large-scale image recognition," arXiv preprint arXiv:1409.1556, 2014.
- [39] R. Mechrez, I. Talmi, F. Shama, and L. Zelnik-Manor, "Maintaining natural image statistics with the contextual loss," arXiv preprint arXiv:1803.04626, pp. 1–16, 2018.
- [40] J. Kim and J. Lee, "Deep residual network with enhanced upscaling module for super-resolution," in 2018 IEEE/CVF Conference on Computer Vision and Pattern Recognition Workshops (CVPRW), June 2018, pp. 913–9138.
- [41] G. Huang, Z. Liu, L. v. d. Maaten, and K. Q. Weinberger, "Densely connected convolutional networks," in 2017 IEEE Conference on Computer Vision and Pattern Recognition (CVPR), Jul. 2017, pp. 2261–2269.
- [42] Y. Tai, J. Yang, X. Liu, and C. Xu, "Memnet: A persistent memory network for image restoration," in 2017 IEEE International Conference on Computer Vision (ICCV), Oct. 2017, pp. 4549–4557.
- [43] L.-C. Chen, G. Papandreou, F. Schroff, and H. Adam, "Rethinking atrous convolution for semantic image segmentation," arXiv preprint arXiv:1706.05587, 2017.
- [44] Z. Tang, S. Li, L. Luo, M. Fu, H. Peng, and Q. Zhou, "Image super-resolution via simplified dense network with non-degenerate layers," IEEE Access, pp. 1–1, 2019.
- [45] Z. Wang, D. Liu, J. Yang, W. Han, and T. Huang, "Deep networks for image super-resolution with sparse prior," in 2015 IEEE International Conference on Computer Vision (ICCV), Dec. 2015, pp. 370–378.
- [46] T. Peleg and M. Elad, "A statistical prediction model based on sparse representations for single image super-resolution," IEEE Transactions on Image Processing, vol. 23, no. 6, pp. 2569–2582, Jun. 2014.
- [47] K. Zhang, W. Zuo, S. Gu, and L. Zhang, "Learning deep cnn denoiser prior for image restoration," in 2017 IEEE Conference on Computer Vision and Pattern Recognition (CVPR), Jul. 2017, pp. 2808–2817.
- [48] M. Bevilacqua, A. Roumy, C. Guillemot, and M.-L. Alberi Morel, "Low-complexity single-image super-resolution based on nonnegative neighbor embedding," in Proceedings of the British Machine Vision Conference. BMVA Press, 2012, pp. 135.1–135.10.
- [49] R. Zeyde, M. Elad, and M. Protter, "On single image scale-up using sparse-representations," in Proceedings of the 7th International Conference on Curves and Surfaces, 2012, pp. 711–730.
- [50] D. Martin, C. Fowlkes, D. Tal, and J. Malik, "A database of human segmented natural images and its application to evaluating segmentation algorithms and measuring ecological statistics," in 2001 IEEE International Conference on Computer Vision (ICCV), vol. 2, Jul. 2001, pp. 416–423.
- [51] J. Huang, A. Singh, and N. Ahuja, "Single image super-resolution from transformed self-exemplars," in 2015 IEEE Conference on Computer Vision and Pattern Recognition (CVPR), Jun. 2015, pp. 5197–5206.

- 705 [52] Y. Matsui, K. Ito, Y. Aramaki, A. Fujimoto, T. Ogawa, T. Yamasaki,  
and K. Aizawa, "Sketch-based manga retrieval using manga109 dataset,"  
Multimedia Tools and Applications, vol. 76, no. 20, pp. 21 811–21 838,  
2017.
- 710 [53] D. P. Kingma and J. Ba, "Adam: A method for stochastic optimization,"  
arXiv preprint arXiv:1412.6980, 2014.
- [54] A. Paszke, S. Gross, S. Chintala, G. Chanan, E. Yang, Z. DeVito, Z. Lin,  
A. Desmaison, L. Antiga, and A. Lerer, "Automatic differentiation in  
pytorch," 2017.
- 715 [55] R. Timofte, R. Rothe, and L. V. Gool, "Seven ways to improve example-  
based single image super resolution," in 2016 IEEE Conference on Com-  
puter Vision and Pattern Recognition (CVPR), Jun. 2016, pp. 1865–1873.

...